Hardware Solutions for High Data Rate Modems

ZHONGXIA (SIMON) HE

Department of Microtechnology and Nanoscience
CHALMERS UNIVERSITY OF TECHNOLOGY
Göteborg, Sweden 2011

Hardware Solutions for High Data Rate Modems

by

ZHONGXIA (SIMON) HE

何 仲 夏

Hardware Solutions for High Data Rate Modems
Zhongxia (Simon) He

This thesis has been prepared using LaTeX.

Department of Microtechnology and Nanoscience
Microwave Electronics Laboratory
Chalmers University of Technology
SE-412 96 Göteborg, Sweden

Phone: +46 (0)31 772 1895
E-mail: zhongxia@chalmers.se

To all the people I love

Abstract

The exponentially-growing mobile data traffic imposes significant demands on the capacity of the mobile network. Fiber optic and microwave links are two main solutions for the mobile backhaul network, which provides connectivity between radio base station (RBS) sites and the switch sites. As compared to fiber, a microwave solution is much easier to deploy, however, its capacity is lower. This thesis is devoted to the design and implementation of modems supporting high data rate transmission.

This thesis includes the design and implementation of one MMIC-based on- /off- keying (OOK) modem and two FPGA-based differential phase shift keying (D-QPSK) modems. The OOK modem is designed for short-distance applications. The D-QPSK modems are made for high capacity microwave radio applications.

The OOK modulator is implemented in a heterojunction bipolar transistor (HBT) process, and is capable of transmitting data at rate of 14 Gbps. The OOK demodulator is implemented in a metamorphic high electron mobility transistor (mHEMT) process with a detection range of 10 to 60 GHz. An OOK link is set up and 10 Gbps transmission is achieved.

For the D-QPSK scheme, a 2.5 Gbps and a 5 Gbps D-QPSK modem are implemented with FPGAs and microwave components. Modifications at the modulator and demodulator are explained, which doubles the data rate of the D-QPSK modem. It also enables the possibility of scaling up to even higher data rates. A point-to-point radio is demonstrated by using such a modem and commercial E-band RF front-end components, which achieves 5 Gbps full-duplex data transmission.

Keywords: OOK, D-QPSK, Mobile Backhaul, Modem, MMIC, HBT, mHEMT, Differential Encoder, FPGA, E-band, Point-to-point Radio.

List of appended papers

[A] Z. He, T. Swahn, Y. Li, H. Zirath, "A 14 Gbps On/Off Keying Modulator in GaAs HBT Technology," submitted to *Microwave and Wireless Components Letters*

[B] Z. He, W. Wu, J. Chen, Y. Li, H. Zirath, "An FPGA-based 5 Gbit/s D-QPSK Modem for E-band Point-to-Point Radios," submitted to *Microwave Integrated Circuits Conference (EuMIC), 2011 European*

[C] H. Zirath, Z. He, "Power detectors and envelope detectors in mHEMT MMIC-technology for millimeterwave applications," *Microwave Integrated Circuits Conference (EuMIC), 2010 European*, pp.353-356, Sept. 2010

[D] Z. He, J. Chen, Y. Li, H. Zirath, "A Novel FPGA-Based 2.5 Gbps D-QPSK Modem for High Capacity Microwave Radios," *IEEE International Conference on Communications (ICC'10)*, pp.1-4, May 2010

Contents

Abbreviations and acronyms

2G	Second generation
3G	Third generation
AWGN	Additive white Gaussian noise
BER	Bit-error rate
BPF	Band-pass filter
CW	Continuous wave
D-QPSK	Differential quadrature phase shift keying
DeMUX	Demultiplexer
FET	Field effect transistor
FPGA	Field programmable gate array
HBT	Heterojunction bipolar transistor
HRAN	Higher radio access network
IF	Intermediate frequency
LPF	Low-pass filter
LRAN	Lower radio access network
LTE	Long term evolution
MMIC	Monolithic microwave integrated circuit
Modem	Modulator and demodulaor
mHEMT	Metamorphic high electron mobility transistor
MUX	Multiplexer
OOK	On- /off- keying
PCB	Printed circuit board
PPL	Parallel prefix layer
PSK	Phase shift keying

QPSK	Quadrature phase shift keying
QoS	Quality of service
RAN	Radio access network
RBS	Radio base station
RF	Radio frequency
ROM	Read only memory
SNR	Signal-to-noise ratio
STM-16	Synchronous transport module level-16
TWA	Travelling wave amplifier
UE	User equipment

Chapter 1

Introduction and Motivation

1.1 Background

The Demand on Mobile Network Capacity

With the emergence of numerous smart mobile devices such as handheld smart phones and net-books, the data usage on mobile networks is growing exponentially. As shown in Fig. 1.1, the mobile data traffic generated is expected to grow more than 45 times by 2015 compared to the end of 2009, and even 380 times by 2020, which corresponds to about 57 Gb per month per average subscriber. The mobile data traffic is mainly generated from "Handset data+VoIP" (such as traditional audio call, SMS and MMS service) and "cellular modem" which supports mobile-based internet access. The figure indicates that an increasing percentage of data traffic would come from the "cellular modem" in the future. This increase in mobile traffic puts a huge demand in mobile communication capacity and quality of service (QoS) in mobile networks. In urban area, the mobile capacity is estimated as 25 $Gb/s/km^2$, assuming an average bit rate of 1 MB/s per user during busy hours, and a typical user density of 25,000 $user/km^2$ in dense urban regions [1].

The Mobile Network Structure

A typical mobile network structure is shown in Fig. 1.2. At the left, there is user equipment (UE), which is wirelessly connected to radio base stations (RBS). With the upgrading of RBSs from 2G (second generation) to 3G (third generation) and LTE (Long Term Evolution), the capacity requirement of the UE-to-RBS link is increased. At the right, there are switch/

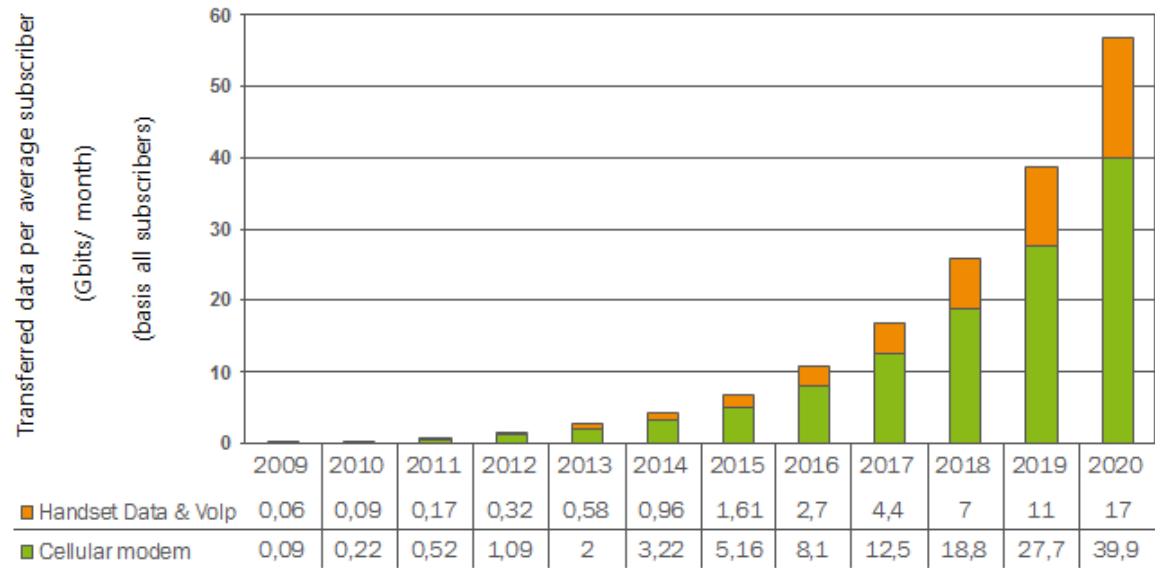|	2009	2010	2011	2012	2013	2014	2015	2016	2017	2018	2019	2020
▪ Handset Data & VoIp	0,06	0,09	0,17	0,32	0,58	0,96	1,61	2,7	4,4	7	11	17
▪ Cellular modem	0,09	0,22	0,52	1,09	2	3,22	5,16	8,1	12,5	18,8	27,7	39,9

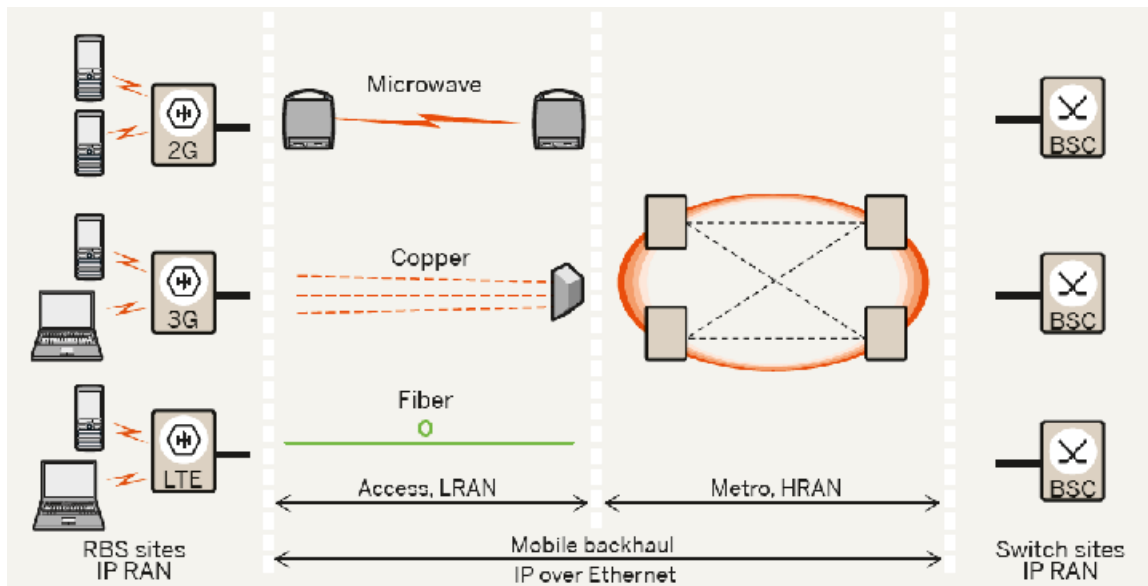Figure 1.1: Growth of transferred data in Western Europe [1]
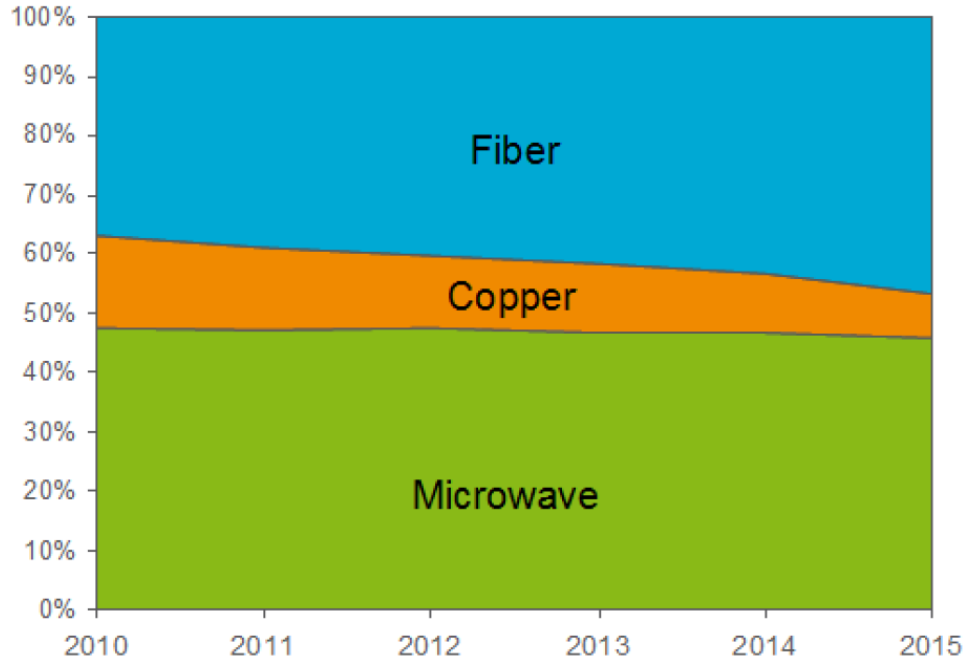

Figure 1.2: A typical mobile network structure

Figure 1.3: The usage forecast for different LRAN solutions [2] [3] [4]

control sites. These sites control the communication between different RBSs and enable the communication between end users of mobile and/or fixed telecom. The links between RBSs and these switch/control sites are called mobile backhaul. The mobile backhaul is an essential part of a radio access network (RAN), which can be divided into two parts: the lower radio access network (LRAN) and higher radio access network (HRAN). HRAN is normally built based on metro ethernet, which is a computer network that covers a metropolitan area and is commonly used as a metropolitan access network to connect subscribers and enterprises to a larger service network or the Internet. The RBSs LRAN need to be connected to nearby nodes in the HRAN; the network links RBSs and HRAN. The distance between RBSs and HRAN nodes is normally several km; this link is also called "last mile" link.

Fiber and Microwave Solutions for LRAN Backhaul

Three solutions are mainly used today for LRAN links: microwave, copper and optical fiber. Fig. 1.3 shows the market share of these solutions. The copper network solution, according to [2], makes up for nearly 20% of all

	Microwave	Fiber
Capacity	Up to several Gbps	Practically unlimited
Regulation	Requires spectrum license	Requires right of ways and infrastructures
Costs and Deployment Time	Cost per link with some incremental cost with the distance. Fast deployment time	Costs and deployment time increase per meter with distance
Terrain	Suitable for any terrain, line-of-sight is required	Costly. Sometime impossible when trenching in difficult terrain (mountains, desert, swamp, etc)
Reuse options	Can be disassembled and relocated	Cannot be reused; Copper ducts may be reused for fibers
Climate	Influenced by climate	No influence, expect for flood and earthquakes, etc

Table 1.1: Solution consideration between microwave and fiber

LRAN deployments, is likely to decrease due to its limited capacity and its inability to scale in a cost efficient manner. Looking forward, fiber is expected to take the place of copper based wire-line connections, and increase its overall share (albeit not at the expense of Microwave).

Currently, microwave and fiber are the main solutions for LRAN. A comparison between these solutions are shown in Tab. 1.1. The main limitation for a microwave solution is its limited capacity compares to the fiber solution. However, the features of fast deployment and ease of relocation makes the microwave solution more attractive than fiber.

1.2   Motivation

Section 1.1 emphasizes the increasing need for high capacity in the mobile network, especially at the RBS sites. Also, we have shown that fiber and microwave links are two main solution for connecting RBS, however, the main disadvantage of the microwave link solution is its limited capacity. It is important to find possible solutions for enhancing the data rate in a microwave link.

In this thesis, hardware solutions for high data rate modulators/ demod-

ulators (modems) are discussed. Two approaches are used for designing and implementing such modems. The first is based on MMIC (monolithic microwave integrated circuit). The other is using FPGA (field programmable gate array) and discrete microwave components.

1.3 Thesis Outline

The thesis is organized as follows: in Chap. 2, we explain the theoretical background, including the concept of passband modulation, spectrum efficiency and detection techniques. Different digital modulation schemes are described as well. In Chap. 3, we focus on the MMIC based OOK modem. We first go through a series of different MMIC OOK modulator design and then a novel structured OOK modulator is introduced. We also present an MMIC based OOK demodulator. The measurement technique we used in measuring this demodulator is described in detail. In Chap. 4, we present two FPGA based D-QPSK modems, for data rates of 2.5 Gbps and 5 Gbps, respectively. The modifications on differential encoding algorithm and demodulator structure are described. These changes are necessary to double the data rate in D-QPSK modem. Finally, conclusions are drawn and ongoing work is presented in Chap. 5.

Chapter 2

Theoretical Background

2.1 Passband Modulation

The basic principle of passband modulation is to encode information into a carrier signal, which is then transmitted over a communication channel [5]. Passband modulation can be categorized as passband digital modulation or passband analog modulation.

In passband analog modulation, the information (i.e. audio) can be represented as a continuous (analog) waveform $S_{info}(t)$. The amplitude $A(t)$, phase $\phi(t)$, and (or) frequency incremental part $\Delta f(t)$ of the modulated signal $S(t)$ are (is) changing with the $S_{info}(t)$ continuously. Thus, the modulated signal can be represented as:

$$S(t) = A(t)sin\{2\pi[f_c + \Delta f(t)]t + \phi(t)\} \tag{2.1}$$

where f_c is the carrier frequency.

In passband digital modulation, information is a stream of binary bits, which can be represented as a discrete sequence $S_{info}[k]$, where k is the index of the sequence. Assuming one symbol contains N bits of data, the symbol stream can also be represented as a discrete sequence $S_{info}[k]$. The passband digital modulated signal can be represented as:

$$S_{[k]}(t) = A[k]sin\{2\pi(f_c + f[k])t + \phi[k]\}, t \in [kT_{sym}, (k+1)T_{sym}) \tag{2.2}$$

Fig. 2.1 depicts the relationship between data bit stream, symbol and modulated signal. Assuming a binary bit $S_{info}[k]$ lasts T_b in time. A symbol, which contains N bits, lasts $T_{sym} = NT_b$ in time. The modulated signal $S(t)$ is a continuous time variant signal, however whose amplitude $A[k]$, phase
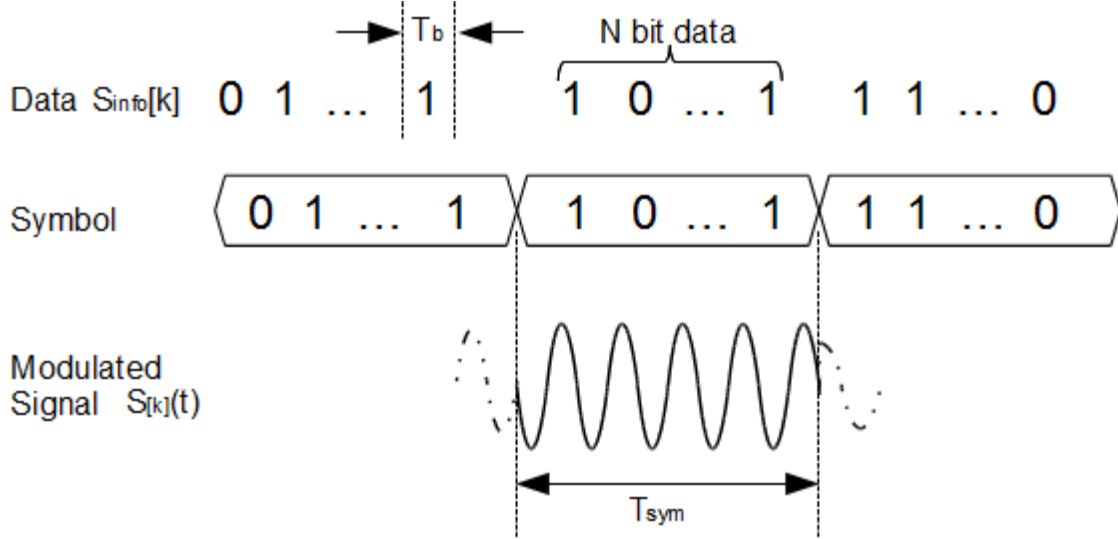
Figure 2.1: A waveform of passband digital modulated signal

$\phi[k]$ and frequency $f[k]$ change discretely according to the symbol $S_{sym}[k]$. Modulation schemes can be divided into amplitude modulation (changing $A[k]$), phase modulation (changing $\phi[k]$) and frequency modulation (changing $f[k]$). Frequency modulation is not popularly for high data rate scenario, because it is difficult to implement, so this thesis focus on only amplitude and phase modulation.

2.2   Amplitude and Phase Modulation

In amplitude and phase modulation, the information bit stream is encoded in the amplitude and/or phase of the transmitted signal. The rule of encoding is called a modulation scheme, which is a mapping between a N-bit symbol and the amplitude and/or phase:

$$[b_0, b_1, ...b_{N-1}] \Longleftrightarrow [A, \phi] \tag{2.3}$$

The expression in Eq. 2.2 can be reformed as:

$$
\begin{aligned}
S(t) &= A[k] \cdot sin(2\pi ft + \phi[k]) \\
&= A[k] \cdot [sin(2\pi ft)cos(\phi[k]) + cos(2\pi ft)sin(\phi[k])] \\
&= A[k] \cdot cos(\phi[k]) \cdot sin(2\pi ft) + A[k] \cdot sin(\phi[k]) \cdot cos(2\pi ft) \quad (2.4) \\
&= Q[k] \cdot sin(2\pi ft) + I[k] \cdot cos(2\pi ft) \\
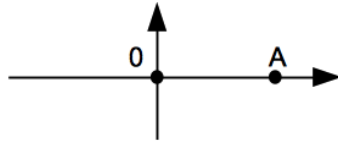&= e^{j2\pi ft + I[k] + jQ[k]}
\end{aligned}
$$

data	modulated signal	constellation diagram
0	0	
1	$s(t) = A sin(2\pi f_c t)$	

Table 2.1: Modulation scheme of OOK

Eq. 2.4 shows that a symbols can be represented as a complex number $I[k] + jQ[k]$, where

$$\begin{aligned}I[k] &= A[k] \cdot sin(\phi[k]) \\ Q[k] &= A[k] \cdot cos(\phi[k])\end{aligned}$$

$$(2.5)$$

It can be visualized as a point on the complex plane. The real and imaginary axes are often called the in phase, or I-axis and the quadrature, or Q-axis. A constellation diagram is a representation of a signal modulated by a digital modulation scheme. It displays the signal as a complex plane scatter diagram in the complex plane. A pack of N-bit data k can be drawn as a point whose coordinates is $[I[k], Q[k]]$. All the possible symbols that may be selected by a given modulation scheme are represented as points in the complex plane. The constellation diagrams of several commonly used modulation schemes are described below:

2.2.1   OOK, BPSK and QPSK

In an OOK scheme, each symbol contains only one bit data. And the data is represented by manipulating only the amplitude $A[k]$. The mapping table and constellation diagram are shown in Fig. 2.1. The advantage of the OOK scheme is that the structure of an OOK modem is simple and easy to implement.

In a PSK scheme, each symbol may contain M bits data. The data is represented by the phase information $\phi[k]$ only, which can be chosen from 2^M possible values. PSK scheme is a constant envelope (constant amplitude) modulation scheme.

In case $M = 1$, the scheme is called BPSK (binary-phase shift keying). Similar as OOK, each symbol contains only one bit data. The mapping table and constellation diagram are shown in Fig. 2.2.

For the case $M = 2$, the scheme is called QPSK (quadrature phase shift keying). Each symbol contains two bits data. The mapping table and constellation diagram are shown in Fig. 2.3.
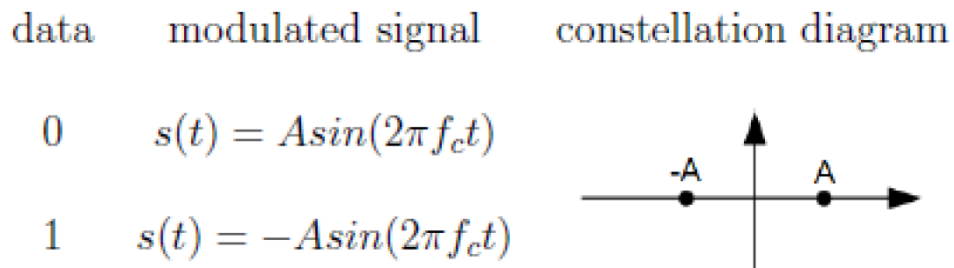
data	modulated signal	constellation diagram
0	$s(t) = A sin(2\pi f_c t)$	
1	$s(t) = -A sin(2\pi f_c t)$	

Figure 2.2: Modulation scheme of BPSK

data	modulated signal	constellation diagram
0 0	$s(t) = sin(2\pi f_c t + 5\pi/4)$	
0 1	$s(t) = sin(2\pi f_c t + 3\pi/4)$	
1 0	$s(t) = sin(2\pi f_c t + 7\pi/4)$	
1 1	$s(t) = sin(2\pi f_c t + \pi/4)$	

Figure 2.3: Modulation scheme of QPSK

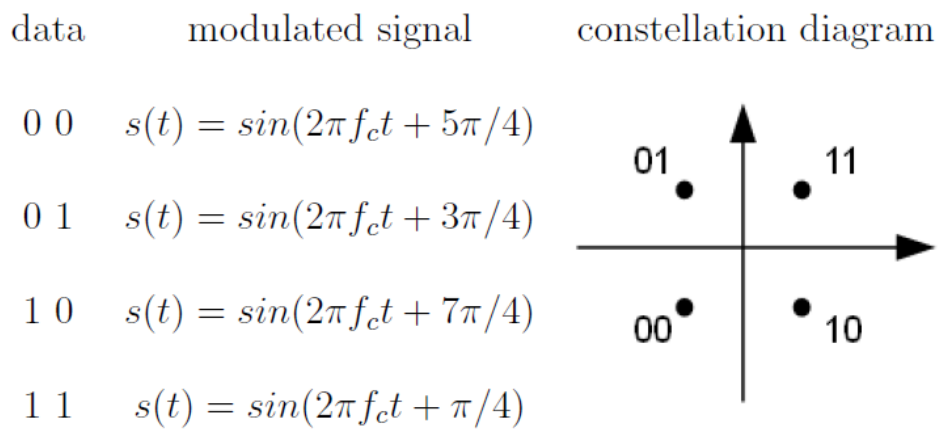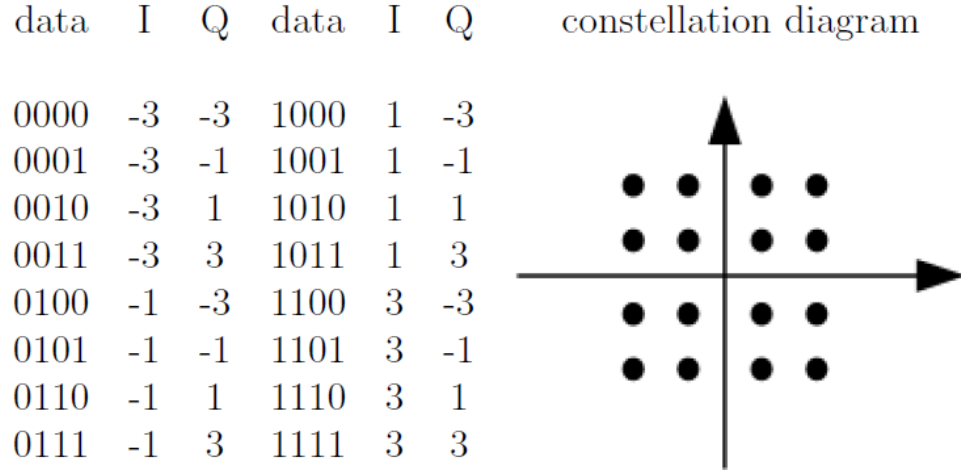| data	I	Q	data	I	Q	constellation diagram
0000	-3	-3	1000	1	-3	
0001	-3	-1	1001	1	-1	
0010	-3	1	1010	1	1	
0011	-3	3	1011	1	3	
0100	-1	-3	1100	3	-3	
0101	-1	-1	1101	3	-1	
0110	-1	1	1110	3	1	
0111	-1	3	1111	3	3	

Figure 2.4: Modulation scheme of QAM

In the general case $M > 2$, there are 2^M symbol states, and each symbol contains M bits data information. However, higher order PSK can tolerate less phase noise than BPSK and QPSK.

2.2.2 Quadrature amplitude modulation (QAM)

Different from the OOK or PSK scheme, a QAM modulation scheme maps a pack of M bit data $[b_{Mk}, ..., b_{Mk+M-1}]$ to both amplitude $A[k]$ and phase $\phi[k]$ of the carrier frequency. By manipulating both amplitude and phase, more bits can be mapped into one symbol. A 16-QAM symbol contains 4 bits data, however, all the possible phase states $\phi[k]$ are not distributed equally. The constellation diagram of 16-QAM are shown in Fig. 2.4.

2.3 Coherent and non-coherent detection

A modulated signal as described by Eq.2.2, received at receiver, can be expressed as:

$$S(t) = A_{path}(t)A[k]sin\{2\pi f_c t + \phi[k] + \phi_{path}(t)\} + N(t) \qquad (2.6)$$

where $A_{path}(t)$ is amplitude attenuation and fading as result of propagation through a certain channel, $\phi_{path}(t)$ is additional phase due to the propagation delay, and $N(t)$ is the noise related to the channel and the transceiver.

An OOK modulated signal can be detected by an envelope detector, which extracts $A_{path}(t)A[k]$. The extracted results can be used as a base for transmitted amplitude estimation.

In the case of phase related modulation (PSK or QAM), demodulation requires good estimation of $\phi[k]$. In other words, the term $2\pi f_c t$ and $\phi_{path}(t)$ must be eliminated. This can be done by two approaches, which are named coherent detection and non-coherent detection.

2.3.1   Coherent detection

Coherent detection is a technique where phase is locked to the carrier signal to improve detection. This phase locking procedure called carrier recovery, in which a reference waveform as $S_{ref}(t) = sin[2\pi ft + \phi_{path}(t)]$ is generated. By comparing the phase difference of the received signal and the reference $S_{ref}(t)$, $\phi[k]$ can be extracted.

2.3.2   Non-coherent detection

The carrier recovery can be a difficult task to implement at high frequency and high data rates. Another detection method which does not require carrier recovery is called non-coherent detection. The principle is to compare the phase difference of two adjacent symbol. Assuming the two samples are taken at t_1 and t_2, which are one symbol period apart: $t_2 = t_1 + T_{sym}$. Both samples can be expressed by Eq. 2.6. The phase difference between these samples is:

$$\angle S(t_2) - \angle S(t_1) = \phi[k+1] - \phi[k] + \phi_{path}(t_2) - \phi_{path}(t_1) + 2\pi f_c(t_2 - t_1)$$
$$= \phi[k+1] - \phi[k]$$

$$(2.7)$$

Where $\phi_{path}(t_2) \approx \phi_{path}(t_1)$, given the channel is line-of-sight point-to-point additive white Gaussian noise (AWGN) channel without multi-path effect.

By comparing the phase of adjacent symbols, the phase difference $\phi[k+1] - \phi[k]$ can be extracted. However, in order to extract $\phi[k]$, the information of the previous symbol $\phi[k-1]$ is still needed. A technique of differential encoding is needed for non-coherent detection. The idea is modulating the data onto the phase difference between adjacent symbols which can be extracted directly by the demodulator. The differential encoding rule is given in the left part of Fig. 2.5. I_k and Q_k are the I and Q signal of the k th symbol. To generate I_k and Q_k, the input data and the state of the $k-1$ th symbol is needed. For example, assume the $k-1$ th symbol is $I_{k-1} = 1$

data	I_k	Q_k	$\Delta\phi$	constellation diagram
00	$\bar{I}_{k-1}$	$\bar{Q}_{k-1}$	180	
01	$\bar{Q}_{k-1}$	I_{k-1}	90	
10	Q_{k-1}	$\bar{I}_{k-1}$	270	
11	I_{k-1}	Q_{k-1}	0	

Table 2.2: The differential encoding rule

and $Q_{k-1} = 1$, given the input data is "10". According to the coding rule, $I_k = Q_{k-1} = 1$ and $Q_k = \bar{I}_{k-1} = -1$. As shown in the right part of Fig. 2.5, an input data "10" would rotate the constellation point 90 degree clockwise.

2.4 Spectrum Efficiency

Spectrum efficiency describes the ability of a modulation scheme to accommodate a given data rate (unit bps) within a limited bandwidth of the carrier (unit Hz) and this therefore has the unit of bps/Hz. The spectrum efficiency values of several commonly used modulation schemes are listed in Tab.2.2. Higher order modulation schemes can support higher data rates; however, a higher bit error probability would be expected at the same signal to noise ratio. The bit error probabilities of various modulation schemes are given [6], by

$$Q(x) = \frac{1}{\sqrt{2\pi}} \int\limits_{x}^{\infty} e^{-y^2/2} dy \tag{2.8}$$

and E_b/N_0 is a normalized signal-to-noise ratio (SNR) measure, also known as the "SNR per bit". E_b is the signal energy received per bit and N_0 is the spectral density of AWGN. Assuming the bandwidth is W and the symbol duration T_{sym}, this yields

Modulation scheme	Data rate	Bandwidth efficiency η	Bit error probabilities [7]
OOK	1.25 Gbps	0.5 bps/Hz	$Q(\sqrt{E_b/N_0})$
BPSK	1.25 Gbps	0.5 bps/Hz	$Q(\sqrt{2E_b/N_0})$
D-BPSK	1.25 Gbps	0.5 bps/Hz	$0.5e^{-E_b/N_0}$
QPSK	2.5 Gbps	1 bps/Hz	$Q(\sqrt{2E_b/N_0})$
D-QPSK	2.5 Gbps	1 bps/Hz	$0.5e^{-E_b/N_0}$
16-QAM	5 Gbps	2 bps/Hz	$0.375Q(\sqrt{2E_b/5N_0})$

Table 2.3: Spectrum Efficiency and Bit Error Probability for common modulation schemes
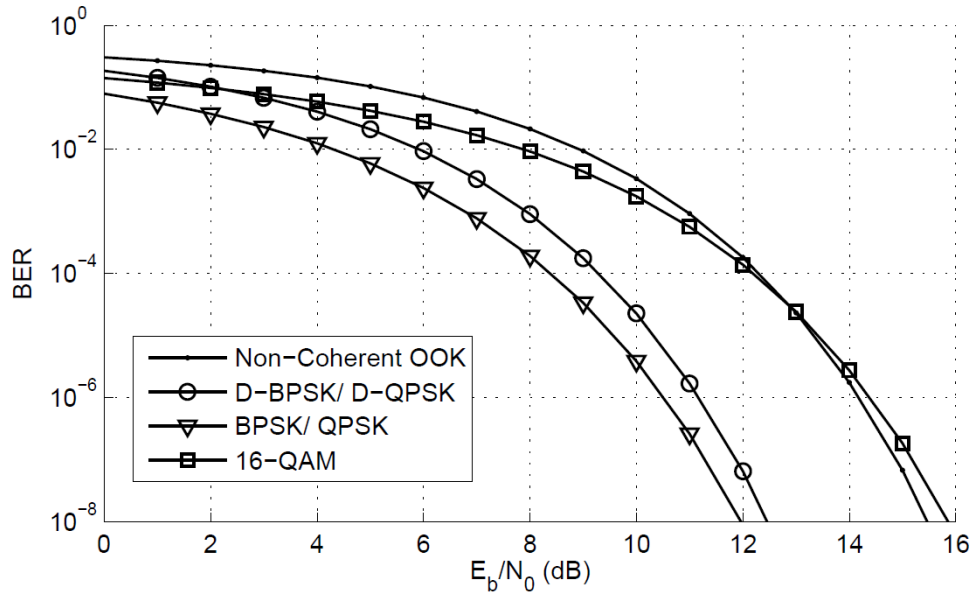
Figure 2.5: The theoretical BER curve of common modulation schemes

$$
\begin{aligned}
SNR = \frac{P_{Signal}}{P_{Noise}} &= \frac{E_b * R_b}{N_0 W} \\
&= \frac{R_b}{W} \frac{E_b}{N_0} \\
&= \eta \frac{E_b}{N_0}
\end{aligned}
\tag{2.9}
$$

where η is the bandwidth efficiency.

The theoretical BER curves of different schemes are plotted in Fig. 2.6. We can see that the best performance of these schemes are BPSK and QPSK with coherent detection followed by D-BPSK and D-QPSK, 16-QAM, and non-coherent OOK. [6]

Chapter **3**

Implementation of OOK Modulator and Demodulator

The OOK modulation has low spectrum efficiency and requires high signal-to-noise ratio to achieve certain BER. The main advantage of this modulation scheme is the simplicity of implementation. In this chapter, different approaches of OOK modulator and demodulator implementations are introduced and discussed.

3.1 MMIC-based OOK modulator

An OOK modulator is, in principle, a device which turns on and off a carrier signal depending on the input data. There are several different structures for building such a functional block. An overview of different OOK modulator solutions are described and discussed as following.

3.1.1 Impulse-radio-type OOK modulator

The concept of an impulse radio provides a method for implementing an OOK modulator without having a carrier generator. A block diagram and operating waveform of an impulse-radio-type OOK modulator are depicted in Fig. 3.1. This modulator is comprised of a pulse generator and a band-pass filter (BPF). The time domain waveform and frequency domain spectrum of the pulse generator output and the BPF output are presented below the block diagram.

The binary data stream ("1011") is input directly to the pulse generator, which generates a narrow pulse when input data is "1". This narrow pulse is
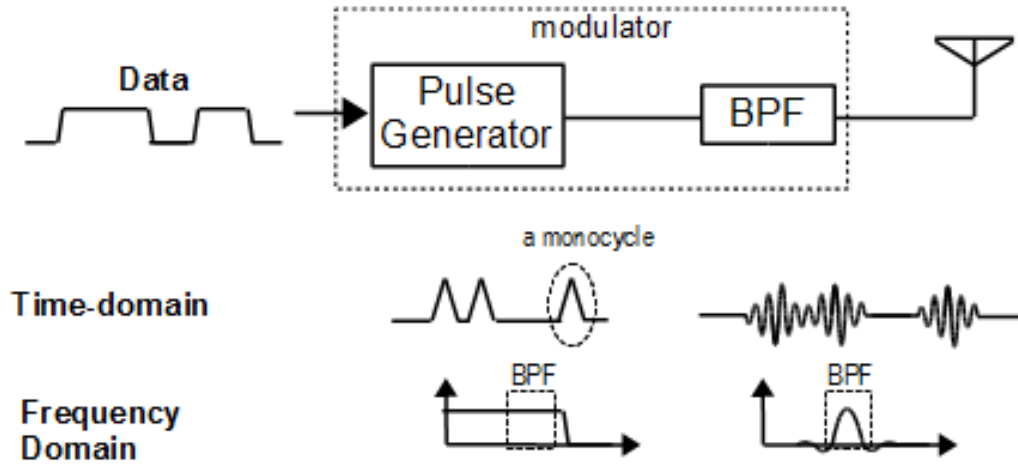
Figure 3.1: The block diagram and waveforms in time- and frequency-domain of a impulse-radio-type OOK modulator

normally referred to as a monocycle [8]. After the BPF, an OOK modulated signal is generated. The time domain waveform of the modulated signal shows high frequency waves (the carrier). This can be explained in the frequency domain. The monocycle occupies a large band in spectrum [9]. By applying a BPF, the energy which is outside of the carrier frequency band of interest is filtered out. The monocycle signal turned into a relative narrow band signal, whose center frequency is defined by the BPF.

The advantage of this structure is that there is no need for a local oscillator. However, in order to transmit signal at a high frequncy (e.g 50 GHz), the pulse generator must be capable of generating a pulse narrower than 20 ps.

3.1.2   RF-Switch-type OOK modulator

Another approach to implement an OOK modulator is using a CW (continuous wave) signal source and an RF-switch, which is controlled by the data. The block diagram of this type of OOK modulator is shown in Fig. 3.2. The important figures of merit of this modulator are the maximum data rate, the insertion loss, the off-state isolation, and the frequency range of the carrier. RF switches can be implemented in different technologies. The preformance of recently-reported OOK modulators are summarized in Tab. 3.1. There are several approaches to implement the switching function. An amplifier can be used as an RF switch, though the range of carrier frequency
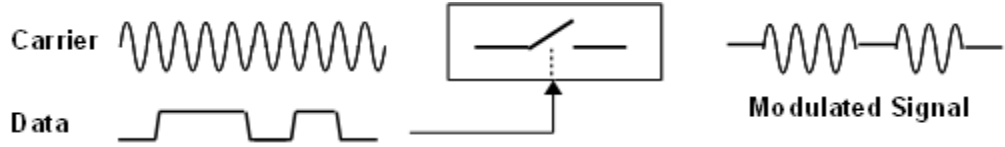
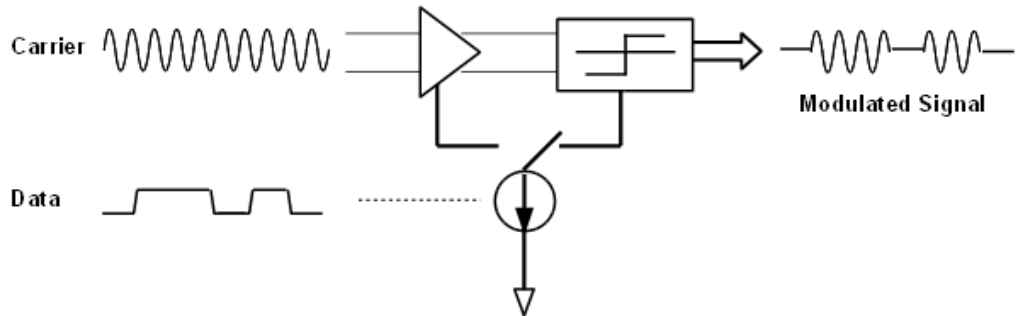Figure 3.2: The block diagram and operating waveform of a RF switch type OOK modulator

Figure 3.3: The function diagram of latch-based OOK modulator

is limited. By switching on and off the DC-supply to the power amplifier, the data can be modulated onto the carrier [10] [11] [12]. For applications which require a wide range of carrier frequencies, a traveling-wave amplifier (TWA) structure would be used [13] [14] [15]. The problem with these solutions is that the off-state isolation is often not sufficient. To improve the isolation, another approach is to switch the carrier oscillator on and off [16]. The data rate, however, is limited due to the time it takes to start up an oscillation. A method of improving isolation is present in [17], in which a differential amplifier is used. At the off-state, the differential output is added to cancel the leakage of carrier. In [Paper A], a new OOK modulator structure is proposed. An emitter-coupled latch is adopted to improve the isolation in the off-state. High data rate is achieved with this circuit than with alternative approaches the other reported.

3.1.3   Latch based high data rate OOK modulator

Referring to Tab. 3.1, an OOK modulator is normally implemented by a field-effect transistor (FET), since a bipolar transistor is not as efficient as a FET device when it is used as a switch. The proposed OOK modulator structure is depicted in Fig. 3.3, which can be implemented in either bipolar or FET

Ref	Technology	Frequency (GHz)	Data rate (Gbps)	Isolation (dBc)	Approach
[10]	90 nm CMOS	60	2	28.4	Switching PA
[13]	90 nm CMOS	60	8	26.6	Switching TWA
[14]	0.4 um FET	DC - 110	1	26.5	Switching TWA
[15]	0.1 um InP HEMT	120	10	20	Switching TWA
[11]	90 nm CMOS	60	2	28.4	Switching Amplifier
[12]	90 nm CMOS	60	2.5	16	Switching Amplifier
[16]	130 nm CMOS	45 - 46	0.15	50	Switching LO
[17]	90 nm CMOS	60	3.5	-	Differential Cancelation
[Paper A]	1.4 um GaAs HBT	DC - 28	14	27	ECL+ latch

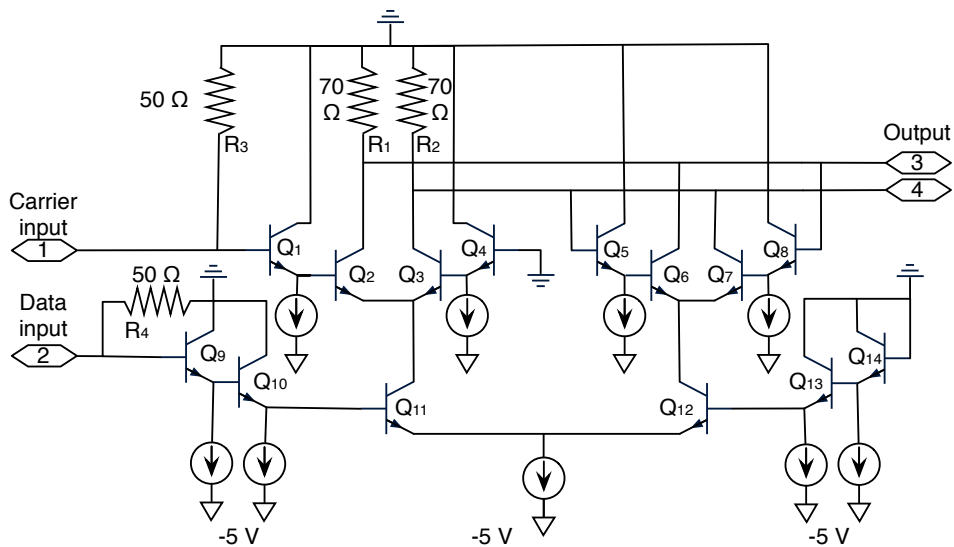Table 3.1: Comparison of previously reported RF-switch-type OOK modulator

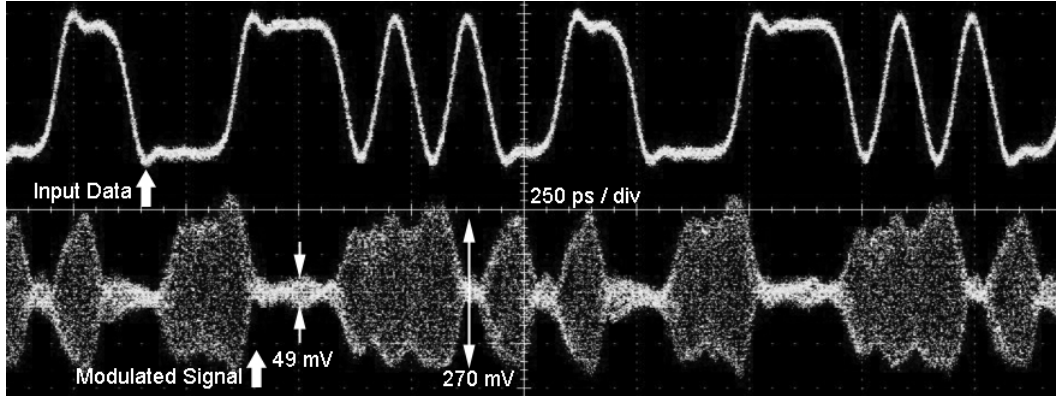Figure 3.4: The schemeticof the proposed OOK modulator

Figure 3.5: Measured time domain waveform of 14-Gbps data modulated on
           a 18-GHz carrier

technology. The modulator contains an amplifier and a latch block. The bias
current through them is controlled by an emitter-coupled pair (ECP) which,
in turn, is controlled by the input data. An RF carrier signal is applied to
the input of the amplifier and the data is applied to the ECP. When the
current supply of the amplifier part is switched on, the modulator is in its
on-state and the carrier is amplified and passed to the output ports. When
the current supply of the latch is switched on, the amplifier block is turned
off and a constant voltage is delivered from the latch to the output port.
The switching function is thus realized by the ECP together with the latch,
eliminating the need for an RF switch.

A proof-of-concept OOK modulator is designed and fabricated in a com-
mercial GaAs HBT process [18]. The HBT device used has a transient fre-
quency f_t=55 GHz and a maximum oscillation frequency $f_{Max} = 63$ GHz.
All HBTs used in this design are single emitter device with emitter size of
1 um $\times$ 10 um. The schematic of the design is shown in Fig. 3.4. $Q_1 - Q_4$
form the amplifier block, and $Q_5 - Q_8$ form the latch block. $Q_9 - Q_{14}$ provide
bias according to the input data. The design requires only a negative 5 V
bias, emitter followers are used to feed signal and provide bias for the next
stages.

To verify the performance of the OOK modulator, both time domain
and frequency domain measurement are carried out. The time domain mea-
surement is to determine the maximum data rate this OOK modulator can
support. In the frequency domain measurement, the maximum carrier fre-
quency this OOK modulator can support can be determined.

Fig. 3.5 shows the measured time domain waveform of an 18 GHz carrier
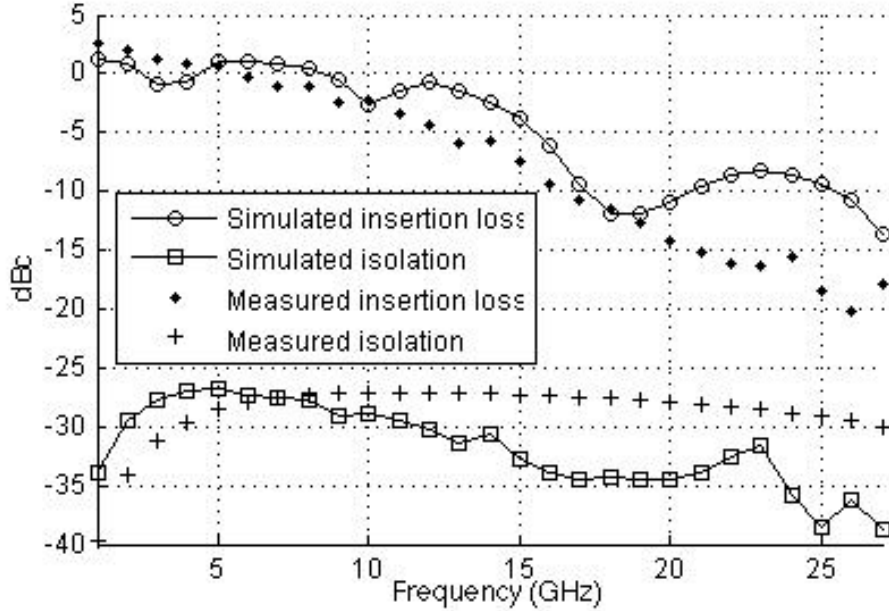signal modulated by a 14 Gbps data signal. The upper waveform is the

Figure 3.6: Measured and simulated of insertion loss and isolation

input data, and the lower waveform is the modulated signal. The peak-to-peak voltage level of the modulated signal at the on- and off- states are 270 mV and 49 mV, respectively, which corresponds to -7.4 dBm and -22.2 dB; a 14.8 dB on- /off- ratio is achieved.

In the frequency domain measurement, a 0 dBm carrier is input, and the output is measured when the data input is keep at logic "1" or logic "0". By changing the frequency of the carrier, the insertion loss (at the on-state) and the isolation (at the off- state) are obtained. The comparison between measurement and simulation is presented in Fig. 3.6. When the 18 GHz carrier is input, the measured insertion loss is -12 dBc and isolation is -27 dBc. This indicates a 15 dB on- /off- ratio, which agrees with the time domain measurement. The frequency domain measurement shows the isolation is better than 27 dB over the operation band. However, a high insertion loss is observed when carrier frequency is larger than 15 GHz. The insertion loss is related to the gain of the differential amplifier. Utilizing inductors as collector loads instead of the resistors R_1 and R_2 may reduce the insertion loss and increase the bandwidth.

Comparing with previously reported results in Tab. 3.1, this design can support a higher data rate while maintaining good isolation.

3.2 MMIC-based OOK demodulator

3.2.1 OOK demodulation solutions

An OOK modulated signal can be demodulated easily using an envelope detector, which can estimate the RF power of the input signal. An envelope detector can be implemented using bipolar [19], Schottky-diode, [20] or FET [21] devices. In [Paper C], we presented two envelope detector designs in a 0.15 μm mHEMT process; one is a Schottky diode passive detector and the other is an active FET detector. The Schottky diode detector has a detection bandwidth from 40 to 60 GHz and a sensitivity of 500 V/W achieved at 60 GHz. The active detector has a wider detection bandwidth from 10 to 60 GHz.

3.2.2 mHEMT active envelope detector

The schematic of the mHEMT based active envelope detector is shown in Fig. 3.7. The modulated signal is input at the gate of a 2 × 20 um mHEMT device through a capacitor C_1 in series with a resistor R_2 (37 Ω). The drain quiescent current I_{DD} is controlled by the gate bias voltage V_{GG}. The drain is connected through R_4 (750 Ω) to V_{DD}. The capacitor C_2 (0.66 pF) is part of the low pass filter (LPF). V_{GG} is normally set near the pinch-off voltage of the device. When there is a cetain RF signal input into the detector, the FET device conducts half cycle of the RF signal, and the LPF slowly follows the envelope of the RF signal, which gives a voltage drop from V_{DD}. When there is no RF signal input, the device is close to pinch-off and the output is nearly V_{DD}. The characteristic of the active detector was simulated as a function of frequency and bias conditions. The optimum bias is $V_{DD} = 2V$ and $I_{DD} = 200\mu A$.

3.2.3 Detector measurement

The transfer function of the detector can be characterized by Eq. 3.1,

$$V_{out} = V_{DD} - f(P_{in}) \qquad (3.1)$$

where $f(P_{in})$ is a Quasi-linear monotonically increasing function. The most straghtforward approach to measure $f(P_{in})$, is to measure the output DC with a certain RF input signal. For low RF-powers, the output of the detector can be characterized by a lock-in amplifier.
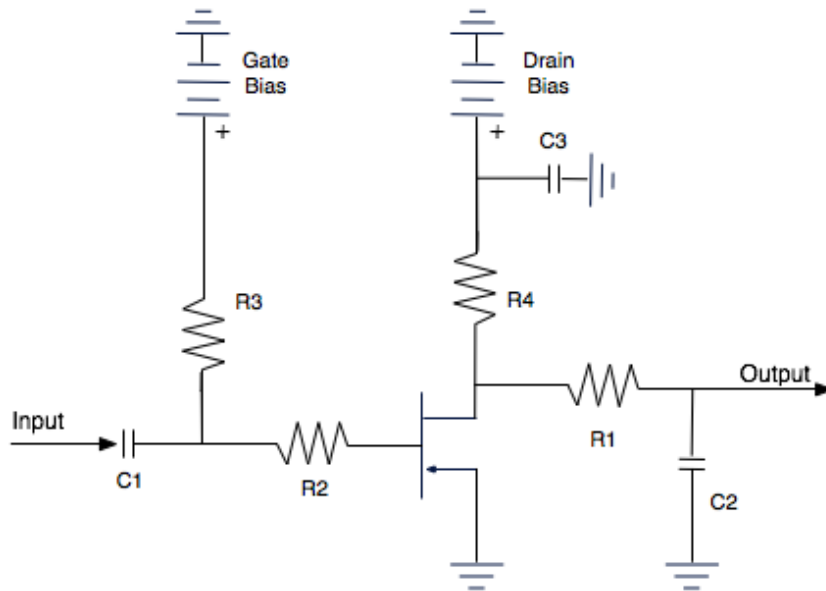
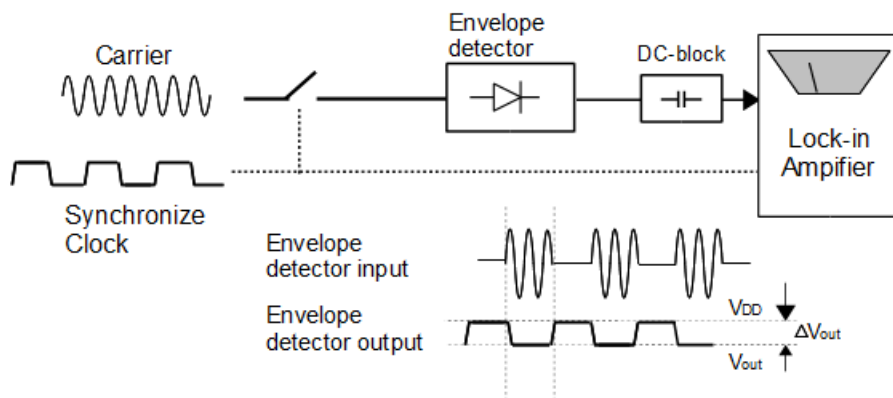Figure 3.7: The schematic of the mHEMT based active envelope detector

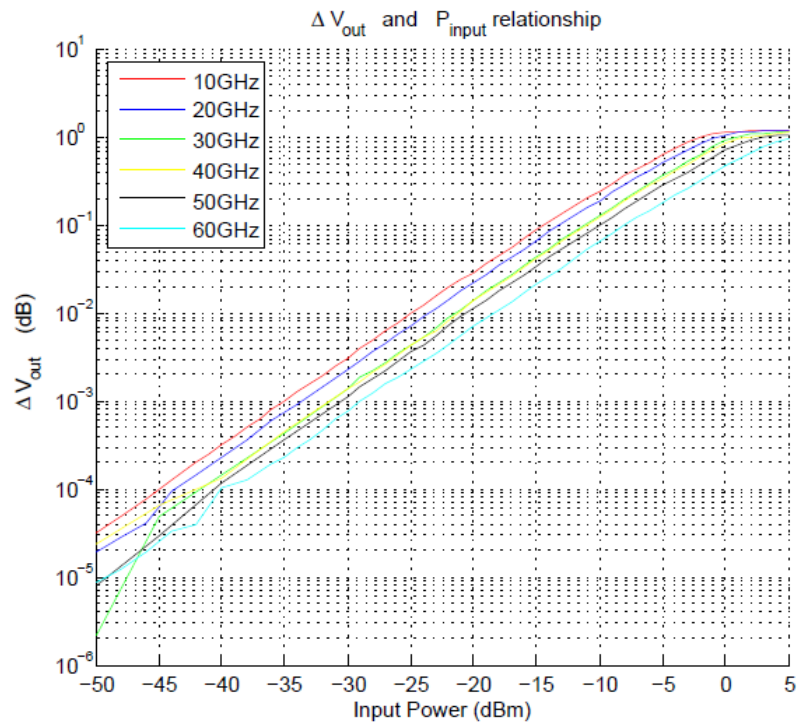Figure 3.8: The measurement setup for the envelope detector

Figure 3.9: Output incremental voltage as a function of input power and frequency
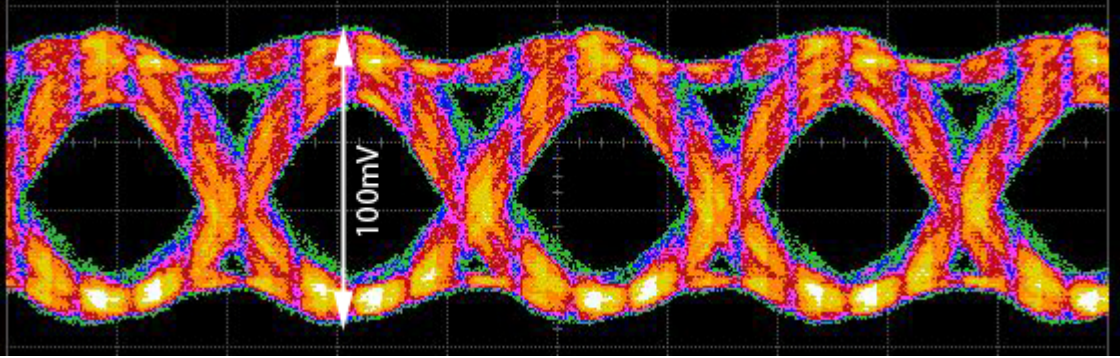
Figure 3.10: Eye diagram of the demodulated signal

The measurement setup is shown in Fig. 3.8. An RF carrier with a certain frequency and power P_{in}, is input to an RF switch, which switches on- and off- under the control of a synchronization clock (around 1 kHz, which is the maximum synchronization rate of the instrument). Thus, the output of the detector is a square wave whose highest voltage is V_{dd}, and lowest voltage is related with the input power. Instead of measuring V_{out}, we now measure ΔV_{out} and its relationship with ΔP_{in}. The lock-in amplifier measures the detector output with the synchronization clock as an additional input. By averaging the output according to the timing indicted by the synchronization clock, it can measure the peak-to-peak voltage of a signal down to uV level. The measurement result of the envelope detector is plotted in Fig. 3.9. The measurement shows linear operation from the lowest power up to -10 dBm, and the detector operates from 10 GHz up to 60 GHz. The maximum sensitivity at 20 GHz is 2800 V/W.

3.3   OOK link modem test

A 10 Gbps data signal is modulated on a 24 GHz carrier using the modulator described in [Paper A] and the active envelope detector [Paper C] is used for demodulation. Fig.3.10 shows the eye diagram of the demodulated signal. The eye opening is 100 mV in amplitude with clear transition, which indicates a good signal quality.

Chapter 4

Implementation of D-QPSK modem

4.1 D-QPSK modulator

4.1.1 2.5 Gbps D-QPSK modulator

The coding rule of the differential-QPSK is shown in Tab. 2.5. This indicates that the signals of I and Q are generated according not only the input data, but also to the previous state of the I and Q signals. A possible implementation of a D-QPSK modulator is shown in Fig. 4.1. The input data are packed into 2-bit groups, the differential encoder takes the states of the I and Q signal and changes them based on the 2-bit input data according to the coding rule. Then the new I and Q signals are generated which would be modulated onto a IF (intermediate frequency) by two mixers. This topology has the limitation that the symbol delay component can be difficult to implement on a PCB (printed circuit board), especially for a data rate higher
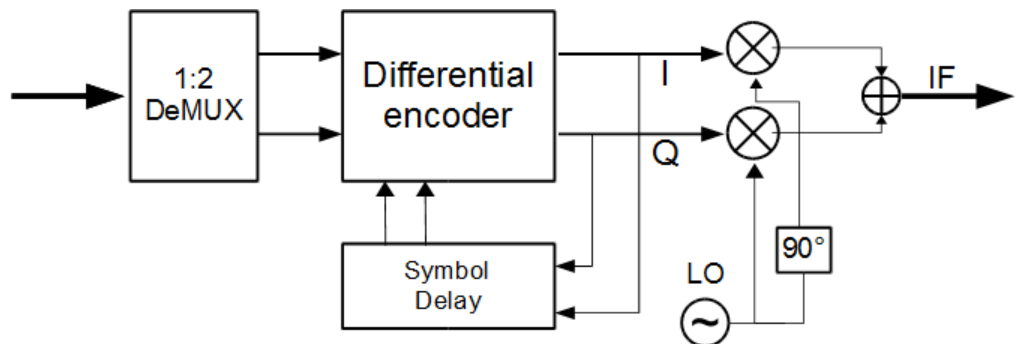

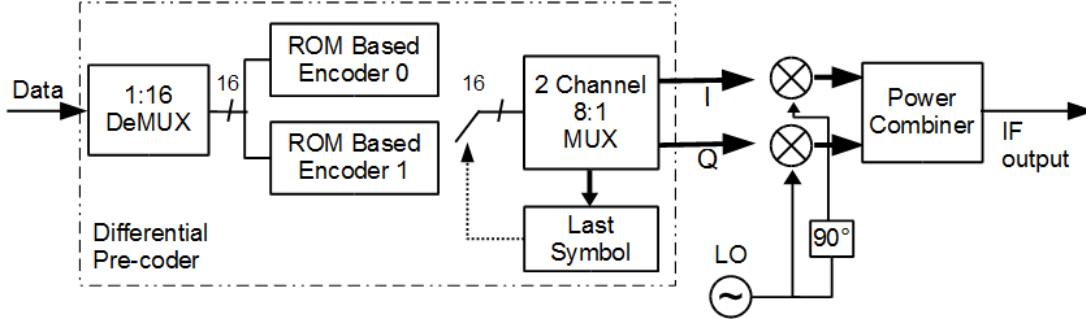Figure 4.1: A topology of the D-QPSK modulator

Figure 4.2: A topology of the FPGA based 2.5 Gbps D-QPSK modulator

than 2.5 Gbps. At the data rate of 2.5 Gbps, the symbol delay is 800 ps. In this topology, I, Q, $\bar{I}$ and $\bar{Q}$ need to be fed back to the encoder via four paths with identical length. This is hard to achieve on a PCB design. To solve this problem, an FPGA based 2.5 Gbps D-QPSK modulator is proposed in [Paper D], where there is no need for feedback. The topology of this modulator is shown in Fig. 4.2. In this topology, a 1:16 DeMUX is used to split the high speed serial stream into lower speed data groups. The feedback path is replaced by a switch, which is controlled by a 2 bit memory cell (storing last symbol information). The differential encoder is implemented by two ROMs (read-only memory) which store the encoded output for all possible inputs. This topology is proven to work at 2.5 Gbps data rate, however, at higher data rates, a DeMUX with wider output bit-width is needed, and the input bit-width of the ROM would be increased correspondingly. Thus this topology is not data rate scalable, due to limited ROM resources in an FPGA.

4.1.2   5 Gbps D-QPSK modulator

To increase the data rate, a new method for differential encoding needs to be developed. The function of the encoder can be described mathematically as:

Assuming a 1:20 DeMUX is used in the high speed differential encoder, a group of 20-bit input data $[b_0, b_1, ..., b_{19}]$, is divided into 10 groups of 2-bit symbol, $[sym_0, sym_1, ..., sym_9]$. According to the differential coding rule, the symbol information is converted as carrier phase difference between two adjacent symbols $[\Delta\Phi_0, \Delta\Phi_1, ...\Delta\Phi_9]$. Assuming that the initial carrier phase is Φ_{int}, then the k-th carrier phase is given by:
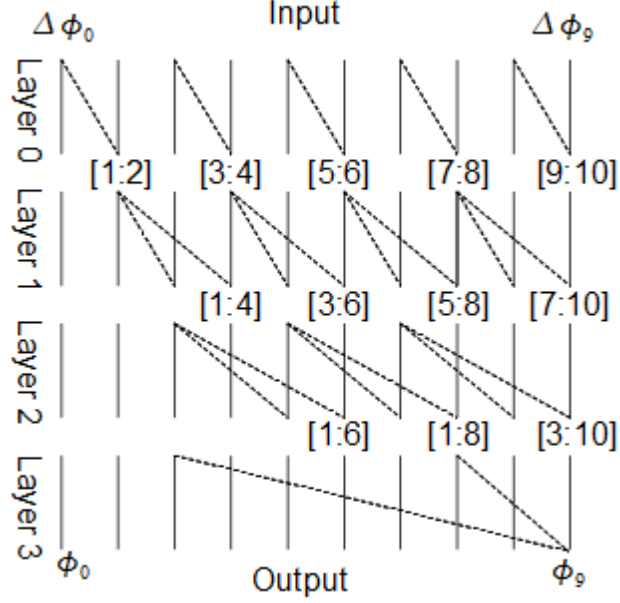
Figure 4.3: Structure of the PPL differential encoder

$$\Phi_k = \Phi_{int} + \sum_{i=0}^{k} \Delta\Phi_i \tag{4.1}$$

where $\Delta\Phi_i \in [0.5\pi, \pi, 1.5\pi, 0]$ and each Φ_k represents a group of $I_k, Q_k \in [-1, 1]$. In [Paper B], we proposed an improved algorithm, called parallel prefix layer (PPL), which can increase the speed of calculation, thereby saving operation time and hardware resources. The principle of the PPL is that the calculation is divided into several steps. In the earlier calculation steps, some "intermediate" calculation results are generated. These results are reused in later calculation steps. The results which are frequently used are calculated in high priority. By sharing such intermediate results, repetitive calculation is avoided, thus the encoding process is more efficient.

The structure of the PPL is depicted in Fig. 4.3. The phase difference data $[\Delta\Phi_0, \Delta\Phi_1, ...\Delta\Phi_9]$ are input from the top. The outputs are obtained at the bottom of the PPL. To calculate 20-bit output (10 symbols), a four-layer PPL is needed. In Fig. 4.3, a notation is introduced, at the bottom of each layer, as:

$$[n, m] = \sum_{i=n}^{m} \Delta\phi_i \qquad\qquad\qquad (4.1)$$

i.e. in layer 1, [1:4] represents the phase-sum: $\sum_{i=1}^{4} \Delta\Phi_i$. We will continue using this notation in the following text, instead of the mathematic expression.

To explain how the PPL works, we take the calculation of Φ_9 as an example. According to Eq. 4.1, Φ_9 requires adding up 10 terms. At layer 0, at odd nodes, input data simply passes through; at even nodes, the sum of two inputs are obtained as intermediate results, such as [1:2], [3:4], ... , [9:10]. At layer 1, [1:4] and [5:8] are calculated by combining some of the outputs of layer 0. At layer 2, [1:8] is calculated and in layer 3 this value would later combine with $\Delta\Phi_9$ and Φ_{int}, thus the final output is obtained at the output of layer 3. The intermediate results in the middle layers are shared for calculating different outputs. Φ_9 is obtained at the final layer, but other output can be generated by passing through only 1 or 2 layers. For instance, the output of Φ_8 can be obtain at the output of the second layer.

The PPL-based modulator structure is plotted in Fig. 4.4. The data are first converted into the form of phase differences $\Delta\Phi$, then passed through different layers. Finally the encoded phase data are converted into I and Q data. Each layer has independent registers to store the intermediate results; the register are updated synchronously using a clock which is 1/20 of the data rate. The FPGA embedded DeMUX is designed in a way that the rate of the DeMUX output is slow enough for the internal FPGA logic gates to handle the data stream. As long as the DeMUX can support, there is no data rate limitation using the PPL structure.

4.2   D-QPSK demodulator

As discussed in section 2.3.2, the data information can be detected by comparing phase differences of two adjacent symbols of the received signal. In the case of D-QPSK modulation, two data bits need to be recovered from this detection. The demodulator structure proposed in [Paper D] is presented in Fig. 4.5(a). First, the received signal is split into two branches. In the upper branch, the signal is delayed by one symbol period and is compared with its replica with 45 degree phase shift. A mixer and LPF (low-pass filter) are used as a phase detector. The upper branch gives high output when two
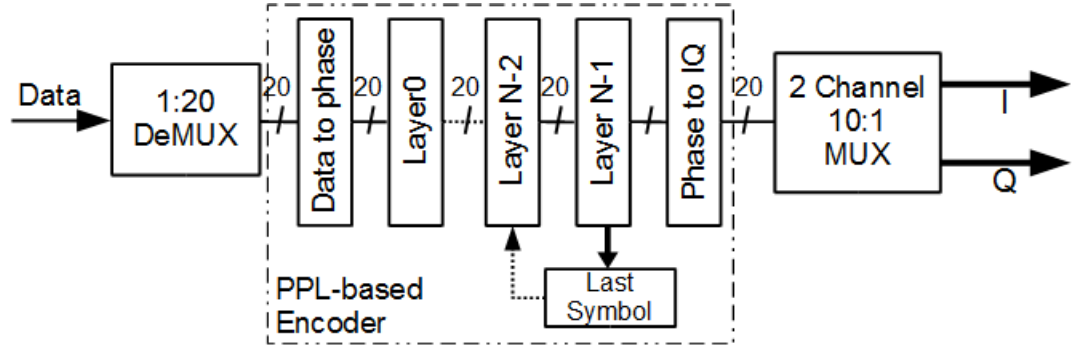
Figure 4.4: PPL-based modulator

adjacent symbols are 0 - 90 degree out of phase; and gives low output when the phase difference is 180 - 270 degree. The lower branch has same structure except a -45 degree phase shift is applied instead of 45 degrees, which gives high output when two adjacent symbols are 270 - 360 degrees out of phase and gives low when the phase difference is 90 -180. The upper branch recovers the second data bit as in Tab. 2.5, and the lower branch recovers the first data bit.

The structure requires two delay elements, which should be identical, and a 45 degree phase shifter is not a standard component. This results in difficulty in setting up such a demodulator. Another demodulator structure is proposed in [Paper B], as shown in Fig. 4.5(b). The improvements are: first, the 45 and -45 degree phase shifters are replaced by a 90-degree coupler which is a standard component; second, two symbol delay elements are combined into one delay element, which eliminates a potential mismatch problem between the two delay elements. In this demodulator, the delay element is tuned to provide a symbol period time delay and 45-degree phase shift at IF frequency. Thus, the structure is equivalent to the one shown in Fig. 4.5(a).
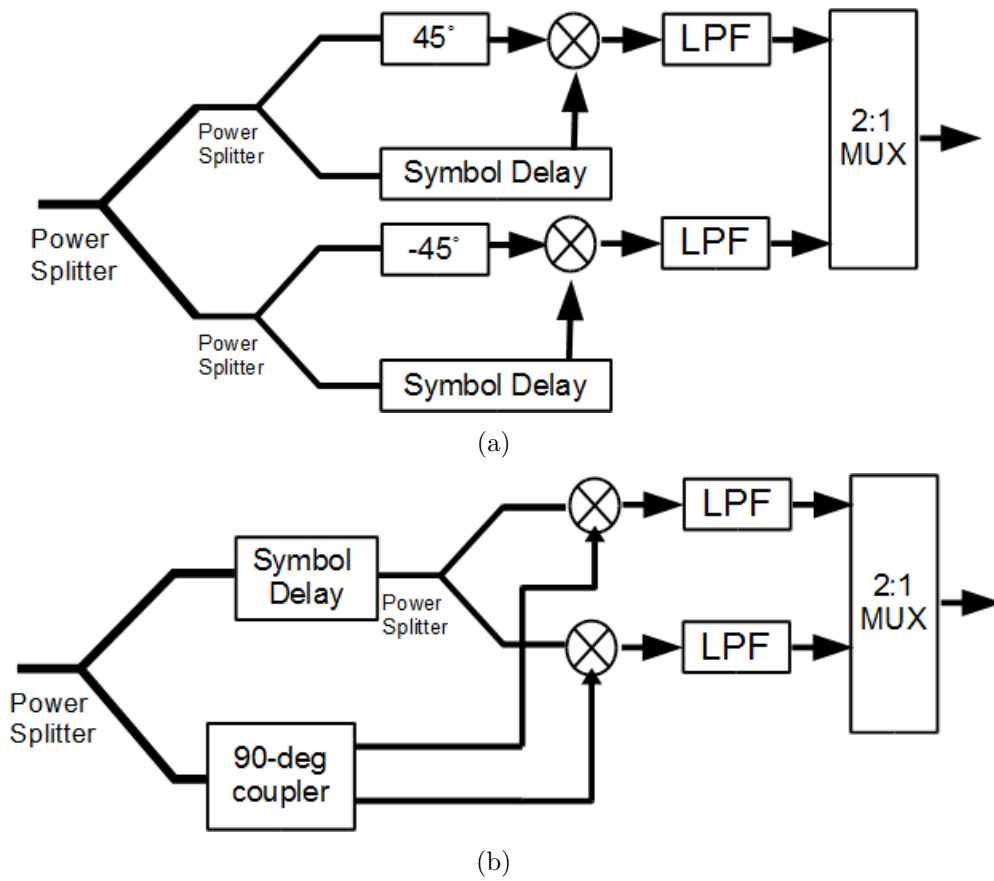
(a)

(b)

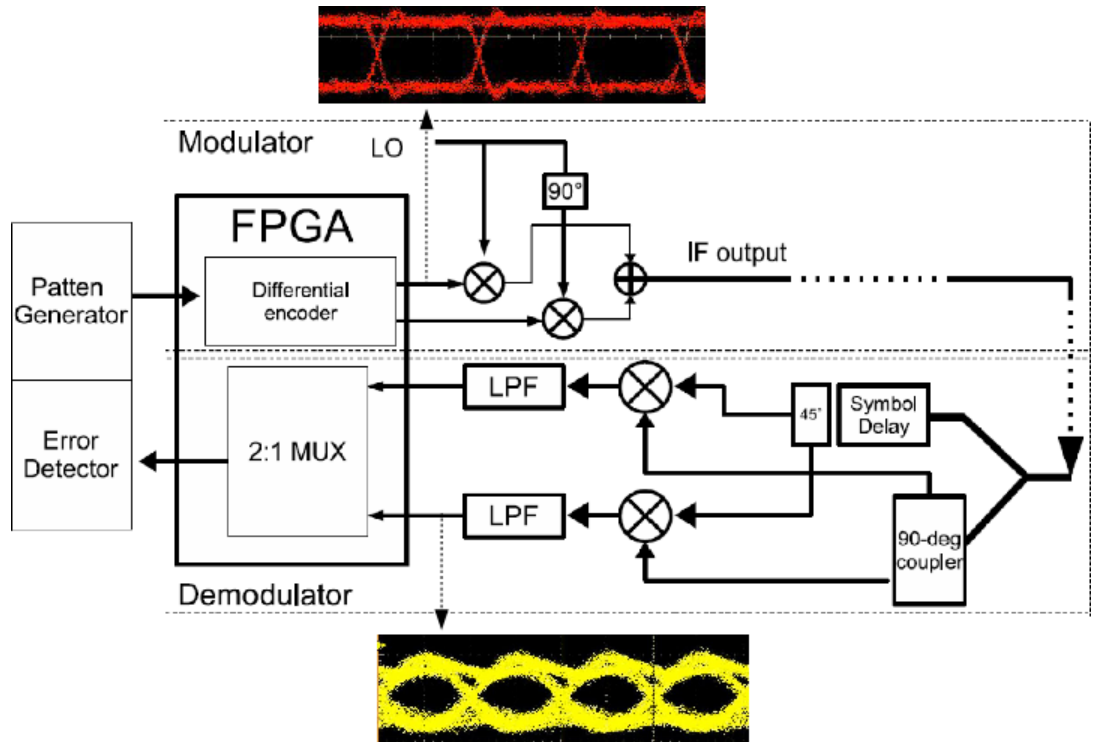Figure 4.5: Alternative implementations of a D-QPSK demodulator

Figure 4.6: The setup of the D-QPSK testbench

4.3 D-QPSK modem test

The setup of the testbench for the D-QPSK modem is depicted in Fig. 4.6.
A pattern generator and an error detector are used to generate data and
verify the bit error performance of the modem. The modulator IF output
is directly connected to the input of the demodulator. The FPGA provides
the differential encoding function as well as the 2:1 MUX function. The LO
signal is provided by a synthesizer, and two mixers are used as IQ modulator.
The waveform of 2.5 Gbaud coded Q output is shown in the upper part of
Fig. 4.6, and the waveform of 2.5 Gbps recovered bit stream from the LPF
output is shown in the lower part.

4.4 5 Gbps D-QPSK E-band Radio

Based on the 5 Gbps modem, a 5 Gbps D-QPSK E-band Radio demonstrator
is implement and tested.

The structure of the full duplex D-QPSK E-band radio is illustrated in
Fig. 4.7(a); the upper part is the transmitter and the lower part is the

receiver. A single fiber operating at STM-16 (Synchronous Transport Module level-16) transmission standard gives 2.488 Gbps data throughput. In the transmitter, two of these fibers are connected to the fiber interface on the FPGA, inside the FPGA these two data streams are interleaved as a 5 Gbps data stream. The differential encoder converts this data stream into I and Q signal, which are modulated onto a 10 GHz IF by an IQ modulator. A commercial E-band module is used to convert the 10 GHz IF signal to the upper (81- 86 GHz) or lower (71- 76 GHz) band of E-band. In the receiver, the E-band module downconverts the RF to an IF signal, and the analog demodulator is used to recover the transmitted data.

A photo of the lab test bench of this radio is shown in Fig. 4.7(b). The radios are connected through a E-band attenuator. The test shows the radio can achieve error-free transmission.
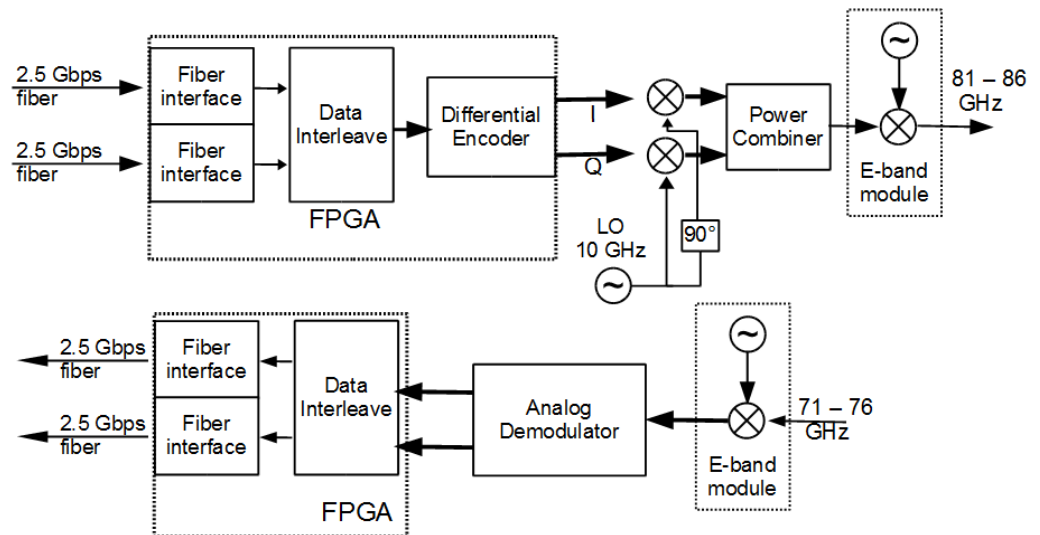
(a) Full duplex D-QPSK E-band radio structure
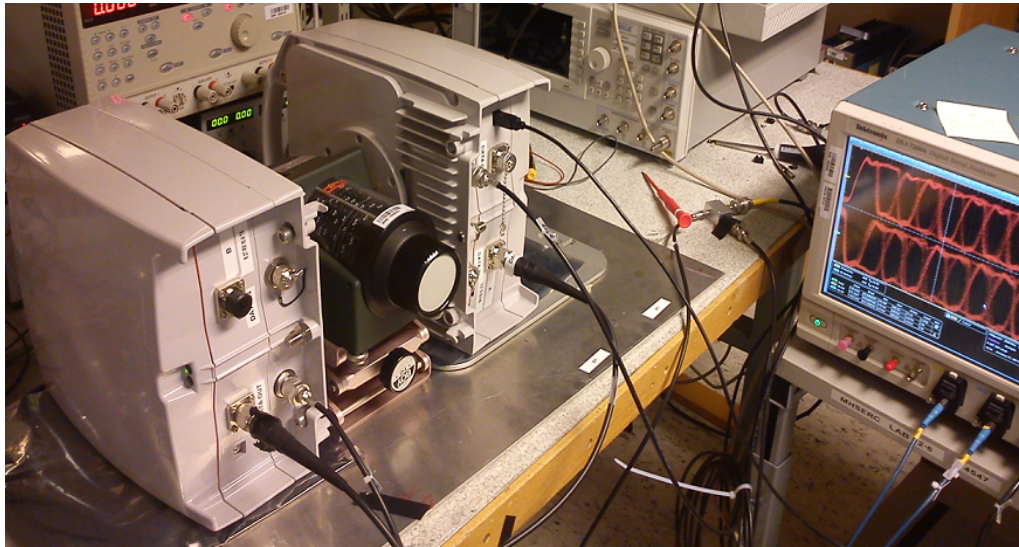
(b)

Figure 4.7: D-QPSK E-band point-to-point radio demonstrator

Chapter 5

Conclusion and Future Work

5.1 Conclusion

This thesis presents design and implementation of high data rate modems for the modulation schemes: OOK and D-QPSK.

An OOK modem is implemented in an MMIC process, and supports over 10 Gbps data transmission. The modem is compact and its power consumption is low. However, to achieve high data rate, a huge RF bandwidth is required. The process used for implementing the OOK modulator has a relative low f_t and f_{Max}, which limits the maximum carrier frequency the modulator can handle. Because of this, this modulator is only a prove-of-concept design. It would be interesting to implement this modulator using a process with higher f_t and f_{Max}, in order to increase the carrier frequency into the mm-wave/ submmwave reigon where bandwidth is huge.

Two FPGA-based D-QPSK modem solutions are also presented in this thesis, which support 2.5 Gbps and 5 Gbps data rate, respectively. These modems are designed and implemented using an FPGA and off-the-shelf microwave components. The 2.5-Gbps D-QPSK modem is a proof-of-concept design, which is practically difficult to scale up to higher data rates. To increase the data rate, modifications are made both on the algorithm and hardware structure. Thus, the 5 Gbps modem can be scaled up to higher data rates. Based on this modem and a commercial E-band module, point-to-point radio for mobile backhaul application is demonstrated. Compared with the OOK modem, the FPGA-based modem is however bulky and consumes much more power.

5.2   Future Work

The presented work in this thesis will be continued in the following directions:

1. Development of a higher modulation scheme
   To achieve 10 Gbps full-duplex transmission on E-band (5 GHz available bandwidth), high order modulation scheme (at least 16 QAM) needs to be used. However, using QAM modulation requires coherent detection. Thus a carrier recovery algorithm needs to be designed and verified.

2. Development of a MMIC-based QPSK modem
   As mentioned above, the FPGA-based modem consumes large amount of power, and the integration level of this solution is low. Implementing a D-QPSK modem in a MMIC process can reduce the power consumption, and the integration level of the design can be increased.

3. Improvements of the MMIC-based OOK modem
   The OOK modulator proposed in this thesis does not operate well at a high carrier frequency. At 120 GHz or 220 GHz, more bandwidth is available, which allows high data rate transmission. It is interesting to explore how well the OOK modem works at these very high frequencies using a cutting-edge MMIC technology.

Acknowlegments

First of all, I would like to express my gratitude to my supervisor, Prof. Herbert Zirath, for giving me the opportunity to embark this journey. Thank you for lighting my path with your guidance, supporting me with your encouragement, and pushing me forward with your enthusiasm.

Also, I would like to thank my co-supervisor Thomas Swahn and Yinggang Li for fruitful discussions, for inspiring explanations, and for being so supportive in both work and personal life.

I owe my thanks to all my colleagues at Microwave Electronics Laboratory. A special thanks to my office mates Lai, Yogesh, Dan, Li-han, Jian and Vessen for creating friendly work environment with lots of laughs and chats. I would like to thank Sten, Marcus and Moretza for being good friends. Also, I want to thank Jonathan for his proofreading and valuable suggestions.

In addition, I would like to thank Thomas Lewin for giving me opportunity to work together with all the colleagues at TLU, Ericsson Research (Mölndal). Espeically, Bengt-Erik Olsson, without your generously sharing of the oscilloscope, work would be thousands times harder. I also appreciate the valuable discussions with Mingquan Bao, Ola Tageman and Jonas Hansryd. Of course, Jingjing, who shared uncountable hours with me in the lab, debugging, tuning, and solving problems, one after another.

And lastly but most importantly, I want to acknowledge my family: My beloved parents who constantly support me as much as they can throughout my life. Also, I'm lucky to have my fiancée Wen with me, who is always understanding and supportive. I would like to thank my friends Tom, My and Joachim as well, for making my life more colorful.

Finally, I would like to acknowledge the Swedish Foundation for Strategic Research (SSF) who has financially supported my stay at Chalmers.

Bibliography

[1] Sheng Liu, Jianjun Wu, Chung Ha Koh, and V.K.N. Lau. A 25 gb/s(/km2) urban wireless network beyond imt-advanced. *Communications Magazine, IEEE*, 49(2):122 –129, 2011.

[2] Heavy Reading Research. Ethernet backhaul quarterly market tracker. 2009.

[3] Tzvika Naveh. Mobile backhaul: Fiber vs. microwave case study analyzing various backhaul technology strategies. 2009.

[4] Alan Weissberger. Ethernet mobile backhaul equipment predicted to spike in 2010 and continue growing. 2010.

[5] A. Goldsmith. *Wireless Communications*. 2005.

[6] Peter Stavroulakis. *Interference Analysis and Reduction for Wireless System*. 2003.

[7] K. Pahlavan and A. Levesque. *Wireless Information Networks*. 2005.

[8] M.Z. Win and R.A. Scholtz. Ultra-wide bandwidth time-hopping spread-spectrum impulse radio for wireless multiple-access communications. *Communications, IEEE Transactions on*, 48(4):679 –689, April 2000.

[9] J. R. Andrews. Picosecond pulse generators for uwb radars. *Picosecond Application Notes*, 2000.

[10] Jae Jin Lee, Chul Woo Byeon, Ki Chan Eun, Inn Yeal Oh, and Chul Soon Park. Gbps 60ghz cmos ook modulator and demodulator. In *Compound Semiconductor Integrated Circuit Symposium (CSICS), 2010 IEEE*, pages 1 –4, 2010.

[11] E. Juntunen, M.C.-H. Leung, F. Barale, A. Rachamadugu, D.A. Yeh, B.G. Perumana, P. Sen, D. Dawn, S. Sarkar, S. Pinel, and J. Laskar. A 60-ghz 38-pj/bit 3.5-gb/s 90-nm cmos ook digital radio. *Microwave Theory and Techniques, IEEE Transactions on*, 58(2):348 –355, 2010.

[12] Fujiang Lin, J. Brinkhoff, Kai Kang, Duy Dong Pham, and Xiaojun Yuan. A low power 60ghz ook transceiver system in 90nm cmos with innovative on-chip amc antenna. In *Solid-State Circuits Conference, 2009. A-SSCC 2009. IEEE Asian*, pages 349 –352, 2009.

[13] A. Oncu, K. Takano, and M. Fujishima. 8gbps cmos ask modulator for 60ghz wireless communication. In *Solid-State Circuits Conference, 2008. A-SSCC '08. IEEE Asian*, pages 125 –128, 2008.

[14] H. Mizutani and Y. Takayama. Dc-110-ghz mmic traveling-wave switch. *Microwave Theory and Techniques, IEEE Transactions on*, 48(5):840 –845, May 2000.

[15] T. Kosugi, M. Tokumitsu, T. Enoki, M. Muraguchi, A. Hirata, and T. Nagatsuma. 120-ghz tx/rx chipset for 10-gbit/s wireless applications using 0.1 mu;m-gate inp hemts. In *Compound Semiconductor Integrated Circuit Symposium, 2004. IEEE*, pages 171 – 174, 2004.

[16] Jri Lee, Yenlin Huang, Yentso Chen, Hsinchia Lu, and Chiajung Chang. A low-power fully integrated 60ghz transceiver system with ook modulation and on-board antenna assembly. In *Solid-State Circuits Conference - Digest of Technical Papers, 2009. ISSCC 2009. IEEE International*, pages 316 –317,317a, 2009.

[17] Hong-Yeh Chang, Ming-Fong Lei, Chin-Shen Lin, Yi-Hsien Cho, Zuo-Min Tsai, and Huei Wang. A 46-ghz direct wide modulation bandwidth ask modulator in 0.13-um cmos technology. *Microwave and Wireless Components Letters, IEEE*, 17(9):691 –693, 2007.

[18] [10] win semiconductor, h01u-00 gaas 1 um hbt model handbook. *Available: http://www.winfoundry.com*.

[19] H.-y.M. Pan and L.E. Larson. A linear-in-db sige hbt wideband high dynamic range rf envelope detector. In *Radio Frequency Integrated Circuits Symposium (RFIC), 2010 IEEE*, pages 267 –270, May 2010.

[20] Seong-Mo Moon, Jong-Won Yu, and Moon-Que Lee. Cmos four-port direct conversion receiver for bpsk demodulation. *Microwave and Wireless Components Letters, IEEE*, 19(9):581 –583, 2009.

[21] Jeongwon Cha, Wangmyung Woo, Changhyuk Cho, Yunseo Park, Chang-Ho Lee, Haksun Kim, and J. Laskar. A highly-linear radio-frequency envelope detector for multi-standard operation. In *Radio Frequency Integrated Circuits Symposium, 2009. RFIC 2009. IEEE*, pages 149 –152, 2009.